JOURNAL OF MATERIALS SCIENCE **36** (2001) 1459–1467

Ultrahigh-temperature deformation of high-purity HIPed Si_3N_4

G. THURN
Japan Science and Technology Corporation (JST), International Cooperative Research Project Ceramics Superplasticity, Japan Fine Ceramics Center 2F, 2-4-1, Mutsuno, Atsuta-ku, Nagoya 456-8587, Japan; Max-Planck-Institut für Metallforschung and Universität Stuttgart, Institut für Nichtmetallische Anorganische Materialien, Pulvermetallurgisches Laboratorium, Heisenbergstr. 5, 70569 Stuttgart, Germany
E-mail: thurn@aldix.mpi-stuttgart.mpg.de

F. WAKAI
Japan Science and Technology Corporation (JST), International Cooperative Research Project Ceramics Superplasticity, Japan Fine Ceramics Center 2F, 2-4-1, Mutsuno, Atsuta-ku, Nagoya 456-8587, Japan

F. ALDINGER
Max-Planck-Institut für Metallforschung and Universität Stuttgart, Institut für Nichtmetallische Anorganische Materialien, Pulvermetallurgisches Laboratorium, Heisenbergstr. 5, 70569 Stuttgart, Germany

High-temperature tensile deformation behavior of high-purity HIPed silicon nitride material was investigated in the temperature range between 1600°C and 1750°C. Recoverable anelastic and non-recoverable deformation was observed in high-purity HIPed silicon nitride. A power-law deformation model analogous to rheological models was used to distinguish the different deformation components. A stress exponent $n = 1.64$ and an activation energy $Q_1 = 708$ kJ/mol was determined for the non-recoverable deformation. For the anelastic deformation a stress exponent $p = 4$ and an activation energy $Q_3 = 619$ kJ/mol was observed. Diffusional creep and grain boundary sliding with the accomodation process responsible for the anelastic component are discussed as deformation mechanisms.

1. Introduction

Silicon nitride ceramics are very important high-temperature structural materials, because of their high strength, moderate toughness, and good creep and oxidation resistance. However, the high-temperature strength, creep resistance and oxidation kinetics depend on the amount and chemical compositions of the additives used for liquid phase sintering [1–3]. The glassy grain boundary phase serves as a path for the diffusion of oxygen and/or gaseous oxidation products. The oxidation kinetics becomes faster with an increasing amount of glassy phase in the material [2]. Transmission electron microscopy investigations showed that silicon nitride grains are always separated by a thin amorphous intergranular film due to the use of additives [4, 5]. The grain boundary phase is liquid at sintering temperature and enhances densification of the covalent silicon nitride materials by a solution-reprecipitation mechanism. However during applications at elevated temperatures, the viscous grain boundary phase also enhances creep by providing regions or paths of high diffusive conductance [6]. It also enables viscous sliding of the grain boundaries and cavity formation, being the major creep mechanisms in liquid phase sintered materials [7, 8]. It was assumed that the viscosity of the intergranular amorphous phase determines the strain rates during creep deformation. Therefore the viscosity of the grain boundary phase in silicon nitride was studied with the technique of internal friction by Mosher *et al*. [9] and a spring-dashpot model for anelastic strain due to grain boundary sliding was suggested. Besides the small viscoelastic strains in internal friction experiments, it was also shown in tensile creep experiments that a considerable amount of the accumulated creep deformation is recoverable strain [10].

To receive a silicon nitride grade with high oxidation and creep resistance, Tanaka *et al*. [11] developed a high-purity silicon nitride grade without sintering aids which was produced by hot isostatic pressing. It was used in previous investigations to study the chemical width of ultrathin amorphous films at grain boundaries [12] and the grain boundary relaxation [13]. Backhaus-Ricoult *et al*. were investigating the compression creep behavior of a similar grade of silicon nitride material and showed that such a high-purity material has a remarkable high-temperature resistance compared to

conventional silicon nitride ceramics [14]. In this investigation it serves as a model material to study the tensile deformation behavior of silicon nitride in the ultrahigh-temperature range between 1600°C and 1750°C.

2. Experimental procedure

The Si_3N_4 material investigated in this study contained only SiO_2 and trace levels of metal impurities but no other additives [11]. The oxygen content of 2 wt % comes from the surface oxidation layer of the powder (SN-E10, Ube Inc., Japan) used for the preparation. The material was hotisostatically pressed (HIPed) for 2 hours at 1950°C under a gas pressure of 180 MPa. The material was fully dense (>99.5%). The silicon nitride grains consist of 100% β-phase with a mean grain size of 1.1 μm. Silica glass was found at triple points and at the grain boundaries. High-resolution electron microscopy (HREM) studies revealed that the layers separating the grains have a thickness of 1 nm [13].

The deformation tests were performed in an 11 bar nitrogen atmosphere in order to prevent thermal decomposition of the silicon nitride. The deformation behavior was investigated in the temperature range between 1600°C and 1750°C. Tests were carried out at constant strain rates (1×10^{-5} s^{-1}, 2×10^{-6} s^{-1}) until a stress between 40 MPa and 100 MPa was reached. Subsequently the stress was kept constant to study creep deformation. The deformation was evaluated from the displacement of the crosshead. Silicon carbide fixtures and pull rods were used to apply the load. After the creep experiments, the specimens were unloaded to observe creep recovery. A clamping force of 2 N was the only load applied during these tests. A dog-bone shaped specimen geometry with a cross section of 0.6 mm × 0.9 mm and a gauge length of 4.4 mm was used for the testing (Fig. 1). The surfaces of the specimens were mirror-polished with diamond pastes.

After the experiments, the microstructure of the materials was investigated by scanning electron microscopy (SEM) and transmission electron microscopy (TEM). For the SEM investigations a Zeiss DSM 982 SEM with a Schottky field emission cathode was used. The specimens were ground, polished and plasma-etched to study the microstructure. With one specimen, energy filtered transmission electron microscope (EFTEM) investigations were carried out using

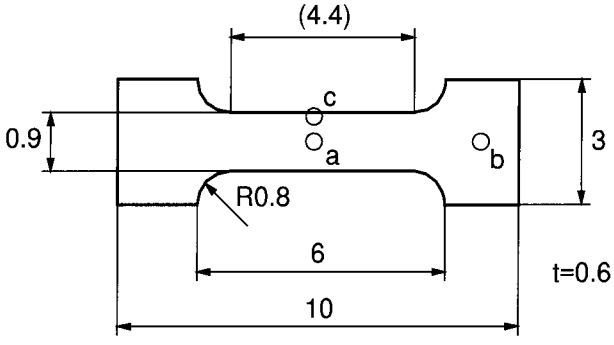

Figure 1 Geometry of the specimens. a, b, and c indicate positions where the microstructure was investigated in the scanning electron microscope.

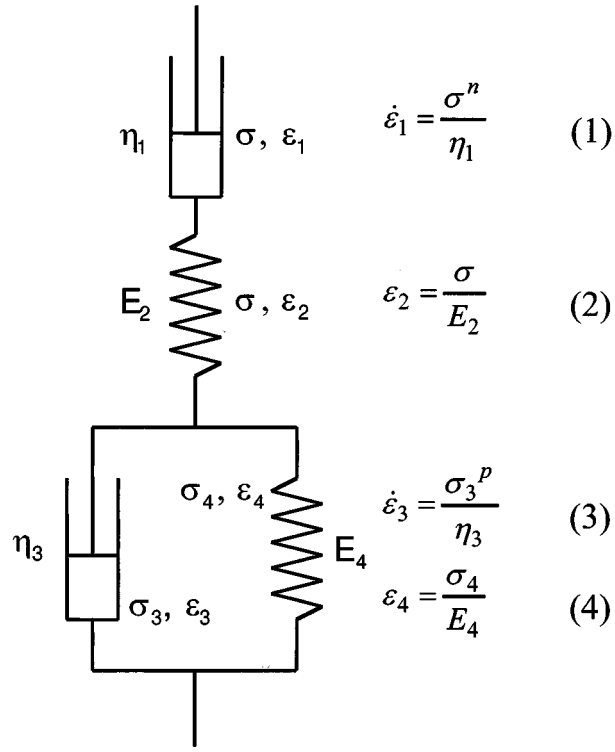

$$\dot{\varepsilon}_1 = \frac{\sigma^n}{\eta_1} \quad (1)$$

$$\varepsilon_2 = \frac{\sigma}{E_2} \quad (2)$$

$$\dot{\varepsilon}_3 = \frac{{\sigma_3}^p}{\eta_3} \quad (3)$$

$$\varepsilon_4 = \frac{\sigma_4}{E_4} \quad (4)$$

Figure 2 Power-law deformation model with constitutive equations, following rheological models.

a Zeiss EM 912 Omega microscope. Standard techniques were used for the preparation of the TEM specimen (grinding, polishing, and ion thinning to electron transparency).

3. Data evaluation

To receive a phenomenological description of the deformation behavior, a power-law deformation model, closely related to rheological models, consisting of elastic, anelastic recoverable and non-recoverable deformation elements was used for data evaluation. The model and the corresponding constitutive equations of the deformation elements are shown in Fig. 2. Power-law relationships between the dashpot stresses and strains were used instead of the linear relationships usually taken for rheological models (Equations 1 and 3). The mathematical description of the circuit of the deformation elements is given by the Equations 5, 6, and 7.

$$\sigma_3 + \sigma_4 = \sigma \quad (5)$$

$$\varepsilon_1 + \varepsilon_2 + \varepsilon_3 = \varepsilon \quad (6)$$

$$\varepsilon_3 = \varepsilon_4 \quad (7)$$

Assuming an Arrhenius relation for the temperature dependence of the dashpot deformabilities, $1/\eta$, the non-recoverable deformation, ε_p, of the model during a creep test with $\sigma = \sigma_0$ is given by a power law relation

$$\varepsilon_p(t) = \frac{\sigma^n}{\eta_1'} \exp\left(-\frac{Q_1}{RT}\right) t, \quad (8)$$

often used to describe the minimum creep rate or the stationary creep behavior of ceramic materials [15]. The

maximum strain of the anelastic part of the model ε_a is determined by E_4. It only depends on the creep stress σ_0 and the temperature T:

$$\varepsilon_{a,\max} = \frac{\sigma_0}{E_4(T)}. \tag{9}$$

The general deformation behavior of the model is given by a partial differential equation derived from the set of the constitutive Equations 1–7:

$$p\eta_3^{-\frac{1}{p}} E_4 \left(\dot{\varepsilon} - \frac{\sigma^n}{\eta_1} - \frac{\dot{\sigma}}{E_2}\right)^{\frac{p-1}{p}} \left[\left(\frac{1}{E_4} + \frac{1}{E_2}\right)\dot{\sigma} - \dot{\varepsilon} + \frac{\sigma^n}{\eta_1}\right] = \ddot{\varepsilon} - \frac{n}{\eta_1}\sigma^{n-1}\dot{\sigma} - \frac{\ddot{\sigma}}{E_2} \tag{10}$$

For the testing conditions, the partial differential equation can be simplified to ordinary differential equations. For constant strain rate tests with $\dot{\varepsilon} = \dot{\varepsilon_0}$ and $\ddot{\varepsilon} = 0$ the evolution of stress can be calculated from

$$p\eta_3^{-\frac{1}{p}} E_4 \left(\dot{\varepsilon_0} - \frac{\sigma^n}{\eta_1} - \frac{\dot{\sigma}}{E_2}\right)^{\frac{p-1}{p}} \left[\left(\frac{1}{E_4} + \frac{1}{E_2}\right)\dot{\sigma} - \dot{\varepsilon_0} + \frac{\sigma^n}{\eta_1}\right] = -\frac{n}{\eta_1}\sigma^{n-1}\dot{\sigma} - \frac{\ddot{\sigma}}{E_2}. \tag{11}$$

For creep tests with $\sigma = \sigma_0$ (= constant) an ordinary differential equation for the deformation is derived

$$-p\eta_3^{-\frac{1}{p}} E_4 \left(\dot{\varepsilon} - \frac{\sigma_0^n}{\eta_1}\right)^{\frac{2p-1}{p}} = \ddot{\varepsilon}, \tag{12}$$

with the solution

$$\varepsilon(t) = \frac{\sigma_0^n}{\eta_1} \cdot t + \frac{\sigma_0}{E_4} - \left[(p-1)\frac{E_4^p}{\eta_3} \cdot t + C\right]^{\frac{1}{1-p}}. \tag{13}$$

The integration constant is determined from the boundary condition $\varepsilon(t=0) = \varepsilon_0$:

$$\varepsilon(t) = \frac{\sigma_0^n}{\eta_1} \cdot t + \frac{\sigma_0}{E_4} - \left[(p-1)\frac{E_4^p}{\eta_3} \cdot t + \left(\frac{\sigma_0}{E_4} - \varepsilon_0\right)^{1-p}\right]^{\frac{1}{1-p}} \tag{14}$$

If the external loads $\sigma_0 = 0$ for the investigation of creep recovery, Equation 12 simplifies to

$$\ddot{\varepsilon} + -p\eta_3^{-\frac{1}{p}} E_4 \dot{\varepsilon}^{\frac{2p-1}{p}} = 0 \tag{15}$$

where

$$\varepsilon(t) = \left[(p-1)\frac{E_4^p}{\eta_3} \cdot t + \varepsilon_0^{1-p}\right]^{\frac{1}{1-p}} \tag{16}$$

is a solution for the boundary condition $\varepsilon(t=0) = \varepsilon_0$. At constant stress experiments, the anelastic strain rate decays. The factor $(p-1)E_4^p/\eta_3$ is the relaxation time constant τ. The higher τ, the faster the anelastic strain rates vanish during the creep tests and stationary creep is observed earlier. The stress exponent p characterizes the time evolution of the anelastic strain rate. The higher the stress exponent, the higher the strain rate changes at the beginning of a stress relaxation.

4. Results

A typical strain vs. time curve for a test at 1750°C and a creep stress of 60 MPa is shown in Fig. 3. The load is applied at a constant strain rate of 2×10^{-5} s^{-1}. A tensile stress of 60 MPa was reached after 15 min. The stress was kept constant and the creep deformation was measured. After approx. five hours, the load was removed quickly and creep recovery was observed. From the load change after the creep test, the stiffness of the testing facility (spring E_2 in the rheological model) was determined. It was shown that the stiffness E_2 can be attributed mainly to the stiffness of the testing machine. The stiffness of the machine was measured temperature-dependent with the fixtures connected directly to each other without specimen. The results are shown in Fig. 4. In these experiments it was also shown that the fixtures only contribute to the elastic and not

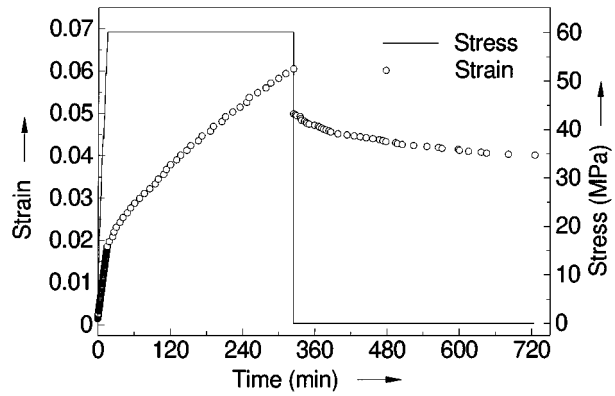

Figure 3 Typical strain vs. time curve for a creep test at a temperature of 1750°C and 60 MPa tensile stress and subsequent creep recovery without mechanical load.

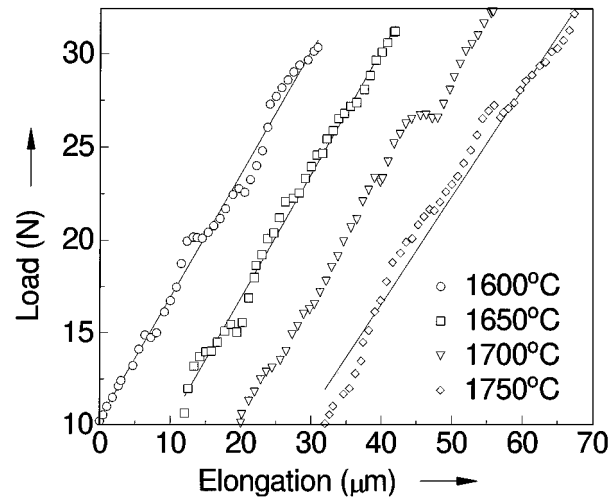

Figure 4 Load-deflection curves from measurements without specimens showing the stiffness of the testing machine.

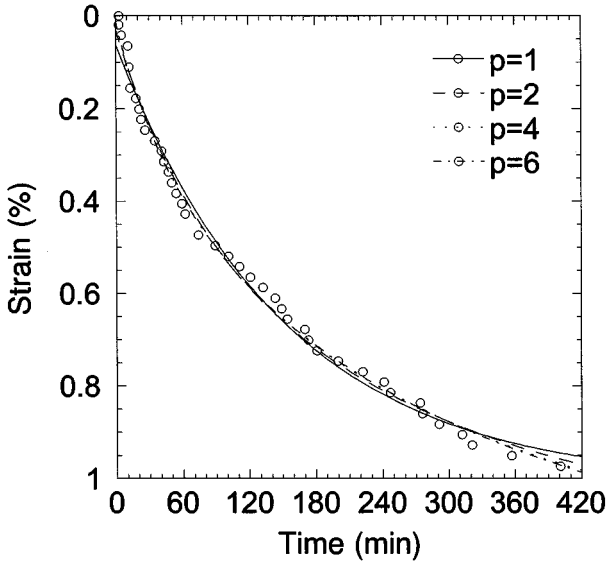

Figure 5 Creep recovery data points after a creep test at 60 MPa tensile stress at 1750°C together with fitted curves calculated from Equation 16 using stress exponents $p = 1$, 2, 4, and 6.

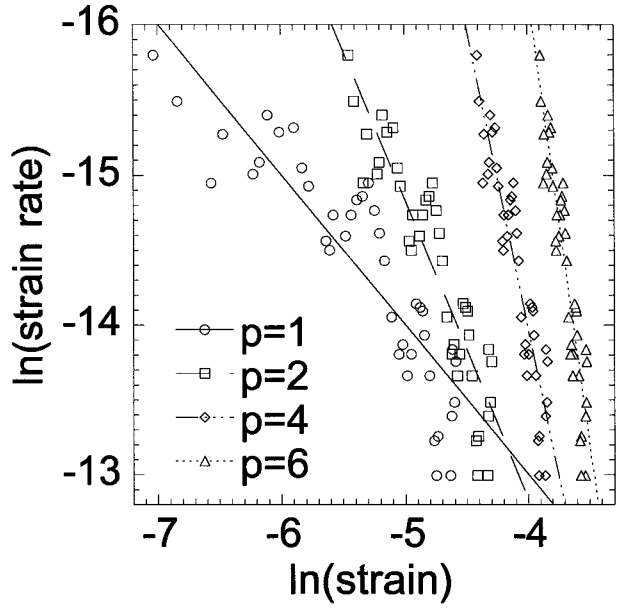

Figure 6 Strain rate vs. strain in double-logarithmic coordinates, showing that different anelastic strains, ε_0, correspond to the assumption of different stress exponents, p.

to the time-dependent deformation. The contribution of the testing machine to the stiffness E_2 is more than one order of magnitude higher than the contribution of the specimens. Due to the scattering of results it was not possible to calculate Young's modulus of the specimen by subtracting the stiffness of the machine from the stiffness E_2 with satisfying accuracy. However, for the evaluation of the constant strain rate experiments with increasing stress, E_2 has to be considered.

During the observation of creep recovery, there is no elastic or non-recoverable contribution to the deformation. The material behavior during creep recovery is then determined by Equation 16 with the relaxation time τ, the stress exponent p, and the initial anelastic strain ε_0 as fit parameters. However, it is not possible to determine three parameters of a creep recovery curve from a single fit. Fig. 5 shows the creep recovery curve after a 60 MPa tensile creep test for five hours at a temperature of 1750°C together with four fitted curves, calculated from Equation 16, using stress exponents $p = 1$, 2, 4 and 6. The relaxation time constant τ and the initial anelastic strain were used as fit parameters. Obviously, the fit with the stress exponent $p = 1$ is not the best fit to the experimental data points. However, it is not possible to decide from the curves which stress exponent p provides the best fit. The major difference between the fitted curves is the initial anelastic strain, which is the limit strain reached after an infinite time. This limit value is $\varepsilon_0 = 1.0\%$ for $p = 1$, $\varepsilon_0 = 1.3\%$ for $p = 2$, $\varepsilon_0 = 2.0\%$ for $p = 4$ and $\varepsilon_0 = 2.7\%$ for $p = 6$. From the physical meaning of the applied model, ε_0 is the anelastic strain stored in the spring 4 at the beginning of the creep recovery experiment. If the creep stress σ_0 is applied for an infinite time before creep recovery, the anelastic strain becomes $\varepsilon_0 = \frac{\sigma_0}{E_4}$ and E_4 can be determined directly from ε_0. However for short time creep experiments, E_4 can only be determined under the consideration of the stress-time history $\sigma(t)$ before creep deformation. Under the assumption that there is no anelastic strain stored in the specimens at the beginning of the constant stain-rate deformation, the accumulated anelastic strain can be determined for an arbitrary stress exponent p

$$\varepsilon_0 = \sum_{t=0}^{t_{CR}} \Delta\varepsilon(t) = \frac{\sigma(t)}{E_4} - \left[(p-1)\frac{E_4^p}{\eta_3} \cdot \Delta t + \left(\frac{\sigma(t)}{E_4} - \varepsilon(t) \right)^{1-p} \right]^{\frac{1}{1-p}} \quad (17)$$

where t_{CR} is the beginning of the creep recovery experiment. This calculation is performed with different deformation parameters E_4 until ε_0 from the stress-time history is in accordance with ε_0 from the fit of the creep recovery curves. From Equation 17 also the anelastic strain at the beginning of the creep deformation ($\sigma_0 = \text{const.}$) can be determined. Knowing this strain, the creep curves can be fitted with the non-recoverable creep strain rate $\dot{\varepsilon}_1$ being the only fit parameter. From the comparison of the creep rates at different stresses, the stress exponent of the non-recoverable deformation can be calculated. When the deformation parameters of the non-recoverable deformation are known, the accumulated non-recoverable strain before the stress relaxation experiment can be calculated. If the calculated accumulated anelastic and non-recoverable strain at the beginning of the creep recovery experiment are not in accordance with the measured strains, the arbitrary chosen stress exponent p was wrong. Several such iterative steps were necessary to determine the stress exponent until consistancy of the model was reached. Fig. 7 shows the calculated stress exponents p and n for different temperatures. For the non-recoverable deformation an average stress exponent $n = 1.64$ was calculated. The average stress exponent of the anelastic deformation was $p = 4$. However, this stress exponent varies somewhat at different

TABLE I Testing conditions and results for the non-recoverable deformation where T is the testing temperature, σ_0 the creep stress, $\dot{\varepsilon}$ the non-recoverable (stationary) strain rate during the creep test, and η_1 the inverse deformability according to the suggested model

T (K)	σ_0 (MPa)	$\dot{\varepsilon}$ (s^{-1})	η_1 (σ in MPa)
1873	70	5.68×10^{-8}	1.87×10^{10}
1873	100	1.01×10^{-7}	1.89×10^{10}
1923	65	3.33×10^{-7}	2.82×10^{9}
1923	80	4.67×10^{-7}	2.83×10^{9}
1973	50	5.31×10^{-7}	1.15×10^{9}
1973	65	7.69×10^{-7}	1.22×10^{9}
2023	40	6.59×10^{-7}	6.43×10^{8}
2023	60	1.45×10^{-6}	5.69×10^{8}

TABLE II Testing conditions and results for the anelastic deformation determined from creep recovery curves, where T is the testing temperature, σ_0 the preceeding creep stress, E_4 the calculated modulus, η_3 the inverse deformability, and p the calculated stress exponent

T (K)	σ_0 (MPa)	E_4 (GPa)	η_3 (MPa^4s)	n
1873	100	14.52	2.25×10^{13}	4.9
1923	65	6.73	5.21×10^{12}	2.3
1923	80	3.28	6.62×10^{12}	4.3
1973	65	3.59	1.87×10^{12}	4.0
2023	60	1.83	1.23×10^{12}	4.1

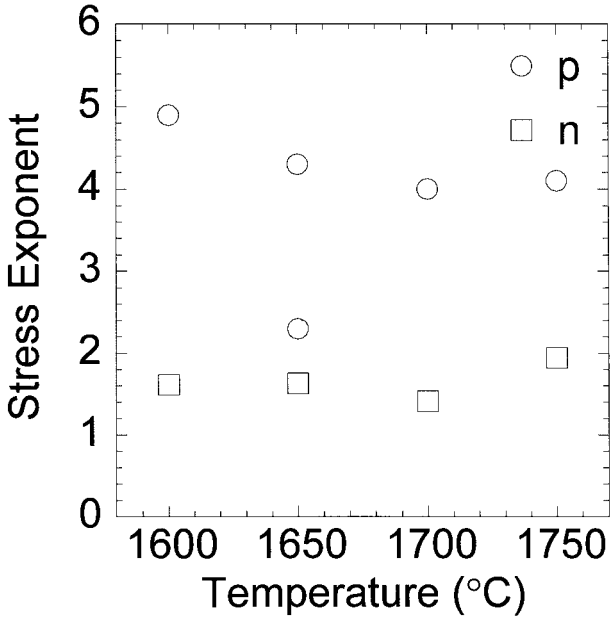

Figure 7 Stress exponent p of the anelastic deformation and stress exponent n of the non-recoverable deformation versus temperature.

temperatures. The results for the non-recoverable deformation are summarized in Table I and the results for the anelastic deformation in Table II. The temperature dependence of the deformabilities $1/\eta_1$ and $1/\eta_3$ is shown in an Arrhenius plot (Fig. 8). An activation energy $Q_1 = 708$ kJ/mol was determined for the non-recoverable deformation and $Q_3 = 619$ kJ/mol for anelastic deformation. The Figs 9 and 10 show creep and creep recovery data for the different temperatures investigated, together with the curves calculated from the proposed model, showing good accordance between the measured data points and the calculated lines.

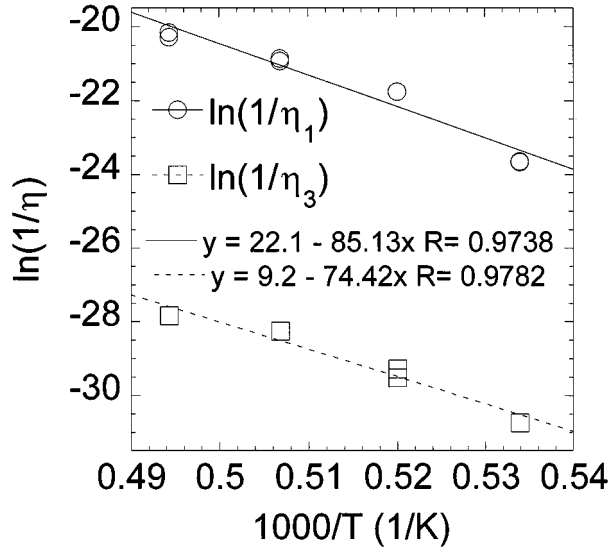

Figure 8 Arrhenius plot of the temperature dependence of the deformabilities $1/\eta_1$ and $1/\eta_3$ of the non-recoverable and anelastic deformation for the determination of the activation energy.

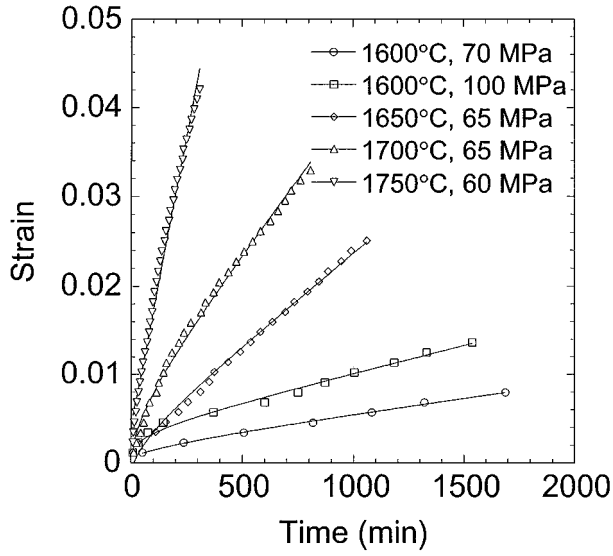

Figure 9 Data points from creep experiments at different temperatures and stresses, together with fitted curves calculated from Equation 14.

To investigate the long-time material behavior a specimen tested for 100 hours at 1873 K was subjected to cyclic loading at a temperature of 1973 K with a stress $\sigma = 70$ MPa at a stress ratio $R = 0$. The strain evolution is shown in Fig. 11. A comparison with the strain evolution during a creep experiment at the same temperature and a stress of 65 MPa shows that the aged specimen has a higher creep resistance, but qualitatively the same deformation behavior as the virgin specimen with non-recoverable and recoverable contributions to the deformation.

5. Discussion

As the specimen size was unusually small for creep investigations, the accuracy of the results was of concern. A creep tests with a bigger specimen size was performed by Luecke [16]. He used a gage length of 16 mm and was able to measure the strain directly at

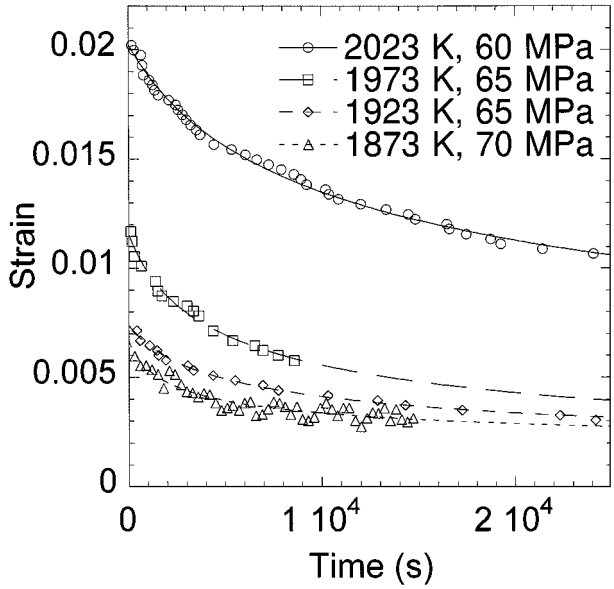

Figure 10 Data points from creep recovery experiments after creep investigations at different temperatures together with fitted curves calculated from Equation 16.

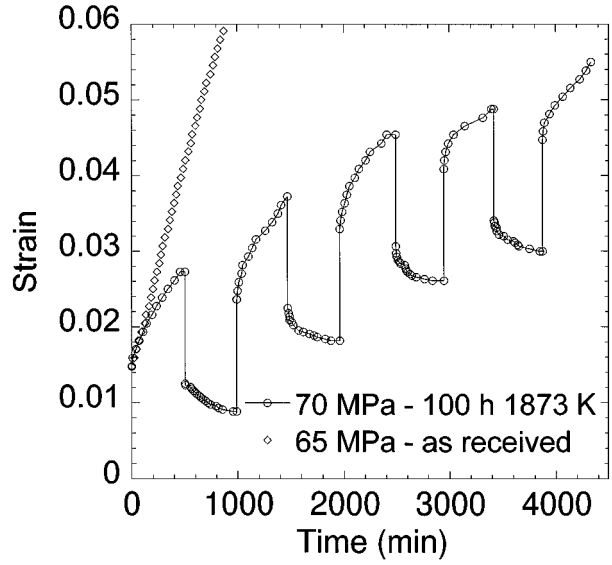

Figure 11 Strain vs. time curve under cyclic loading at a temperature of 1700°C with a repeated stress of $\sigma = 70$ MPa of a specimen which was previously subjected to a 100 hours test at 1873 K. In comparison a creep curve at 1700°C and 65 MPa of an as received specimen is shown.

the specimen, using flags. Due to problems with the preparation of specimens, only a single specimen was obtained for creep testing. The test was performed at 1500°C at a stress of 50 MPa. Because the resolution of the strain measurement system was not sufficient to detect creep deformation, the stress was stepwise increased to 60 MPa and 75 MPa. At 75 MPa a strain of 0.2% was measured within 100 hours. This gives an average strain rate of 5.56×10^{-9} s^{-1}. From the shape of the creep curve, anelastic and non-recoverable could not be distinguished. Due to the stepwise increase of the load, we assume that the anelastic component was too small to be detected. Using the deformation parameters from this investigation a stationary strain rate of 4.89×10^{-9} s^{-1} was calculated for the non-recoverable deformation under those testing conditions. The difference of only 14% between the calculated strain rate and the measured strain rate shows that the accuracy of our measurements is satisfactory.

Two mechanisms contribute to the creep behavior in silicon nitride ceramics. Diffusional creep can be presumed to occur by redistribution of matter through the amorphous grain boundary phase. Solution of Si_3N_4 into the viscous phase and subsequent reprecipitation elsewhere would be driven by differential chemical potentials that arise from localized stresses [17]. The strain rate is related to the grain size (d), molar volume of the diffusing species (Ω), the molar fraction of the diffusing species (C) in the liquid, the volume fraction of the liquid phase (V_1), the viscosity (η) of the liquid, and the applied stress (σ) [17, 6]:

$$\dot{\varepsilon}_{\text{diff}} = \frac{8\Omega^{2/3}}{d^2\eta} C V_1 \sigma \qquad (18)$$

Equation 18 shows that a linear stress dependence of the creep rate is expected, when diffusional creep is the only creep mechanism. If a diffusional creep mechanism is assumed, the creep rate would be controlled by the diffusion coefficient for the slowest species, that is Si [14]. The diffusion of silicon in amorphous silica has been measured by Brebec *et al*. [18]. An activation energy of 579 kJ/mol was found, very close to the activation energy of the plastic deformation $Q_1 = 619$ KJ/mol measured in this study.

The second mechanism involved in the high-temperature deformation of silicon nitride is grain-boundary sliding with accompanying cavitation. The contribution of cavitational creep in comparison to diffusional creep increases with increasing volume fractions of the liquid, higher stresses, longer times and lower viscosity. It is assumed that the temperature dependence of the grain-boundary sliding mechanism is correlated with the activation energy of the viscosity of the grain-boundary phase. The viscosity of the grain boundary phase of the material investigated in this study was measured by Pezzotti *et al*. with internal friction experiments [13]. An activation energy of 410 kJ/mol was found in good correlation with values for transparent SiO_2 (440 kJ/mol) [19] and high-purity SiO_2-glass fibers (390 kJ/mol) [20]. This is significantly lower than in this investigation. It was shown by electron energy losss spectroscopy (EELS) quantitative analytical methods that the grain-boundary films in high-purity HIPed Si_3N_4 ceramics contain a considerable amount of nitrogen [12]. Grain-boundary film compositions of $SiN_{0.49\pm1.4}O_{1.02\pm0.42}$ and $SiN_{0.63\pm0.19}O_{1.44\pm0.33}$ were found in this investigation. It is assumed that the nitrogen concentration in the grain-boundary depends on the time-temperature history and the nitrogen-pressure during the heat-treatment. While the nitrogen pressure in Pezzotti's experiments was only 5 Pa [13], a pressure of 1.1 MPa was applied in our experiment. Therefore we assume that the chemical composition of the grain-boundaries in the two experiments was different. The nitrogen content in [13] was probably lower and therefore the results for the activation energy closer to that of the high-purity SiO_2-glass fibers.

The strain rate for cavitational creep cannot be expressed as a simple power law with respect to time. The stress exponent is between 2 and 7 and increases with stress. For the material investigated, at temperatures between 1600 and 1700°C a stress exponent between 1.41 and 1.63 was found with the higher values determined at higher stresses, indicating that both diffusional and cavitational creep is involved. At 1750°C a higher stress exponent of 1.94 was found, indicating a higher fraction of cavitational creep. SEM micrographs were taken from the tensile loaded (position a in Fig. 1) and the unloaded part of the specimens (position b in Fig. 1). The specimens were tested at 1700°C with an overall strain of 4% (Fig. 12a and b), and at 1750°C with an overall strain of 5.8% (Fig. 13a and b). From Fig. 12 it was concluded that cavitation is not the major deformation mechanism at temperatures below 1750°C. Though smaller cavities may be not visible in the SEM micrographs, an accumulated cavitation volume in the range of 4% should be discovered in the micrographs. Also with the transmission electron microscope cavitation was not observed. However in Fig. 13a it is shown that at 1750°C cavities are produced by separation of two grains perpendicular to their common boundary or by separation of two parts of a broken whisker. As the melting point of SiO_2 is at 1730°C, it is assumed that the lowered viscosity of the grain boundary phase enhanced grain boundary sliding with accompanying cavitation.

According to the model used for the data evaluation, the primary creep deformation is completely recoverable. This is not in general true for all silicon nitride materials. Lange *et al*. [21] observed during tests conducted in air that the strain rates decreased continuously during the test and no stationary creep was attained. He concluded that the oxidation of silicon nitride caused cleaning of the grain boundaries from impurity ions leading to a form of strengthening. A similar kind of strengthening was observed during our experiments with a specimen pre-tested for 100 hours at 1600°C. It is assumed that grain growth during the first experiment caused the increase of the creep resistance. However, due to the small amount of grain boundary phase in this

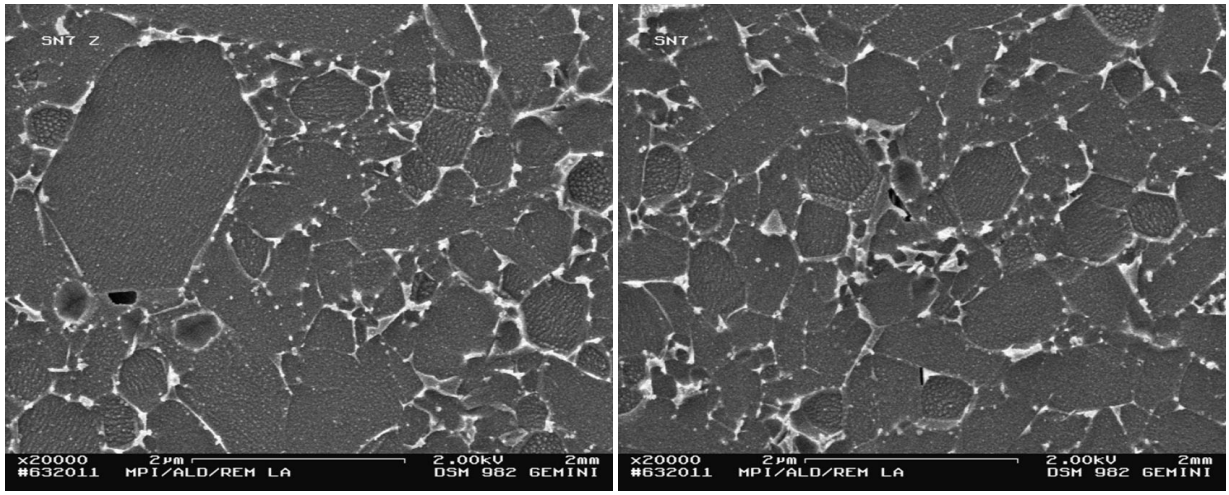

(a) (b)

Figure 12 Microstructure of a specimen tested at 1700°C with an overall strain of 4.0%. (a) Position a in Fig. 1—loaded part; (b) Position b in Fig. 1—unloaded part.

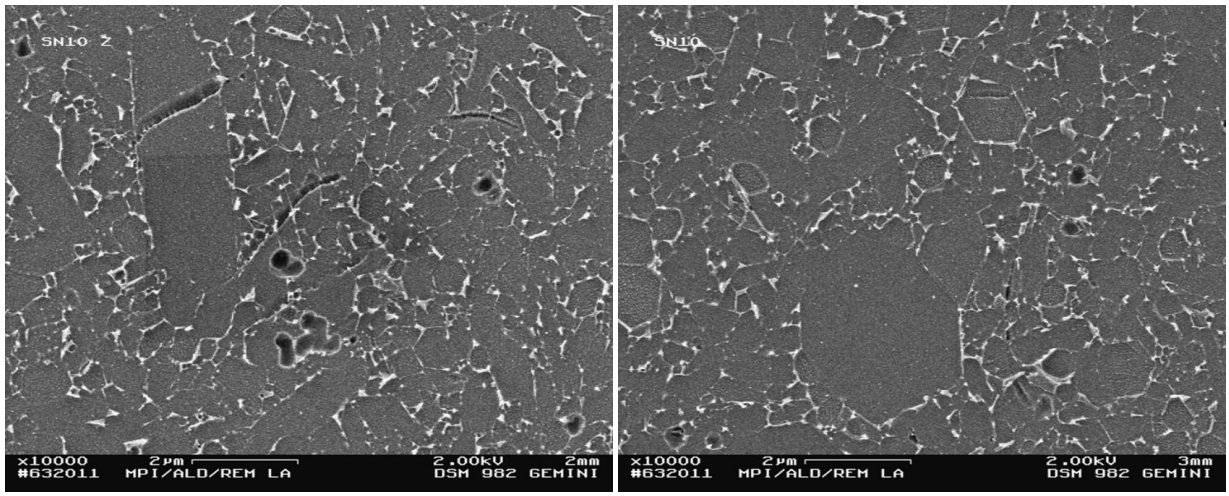

(a) (b)

Figure 13 Microstructure of a specimen tested at 1750°C with an overall strain of 5.8%. (a) Position a in Fig. 1—loaded part; (b) Position b in Fig. 1—unloaded part.

Figure 14 TEM bright field image of the material tested for 100 hours at 1600°C and 72 hours at 1700°C.

material, it is very difficult to make the microstructure visible by either plasma etching or chemical etching. Therefore, changes of the grain size distribution cannot be measured with sufficient accuracy. The specimen tested for 100 hours at 1600°C and for 72 hours at 1700°C was investigated in the analytical transmission electron microscope. Fig. 14 shows the bright field image of the material. There was no sign of cavitation.

Since grain boundaries are usually non-planar, grain boundary sliding must be accompanied by an accomodation process. Small amounts of total sliding can be accomodated by elastic strains in neighboring grains. In this case the strain rate-stress relationship of the anelastic deformation (Equation 3) is linear, i.e., the stress exponent equals $p = 1$. This is the case when a torsional pendulum apparatus is used in internal friction experiments. A spring-dashpot model for the anelastic strain due to grain boundary sliding was suggested by Mosher *et al*. [9] and correlated to the micromechanisms of sliding and mass transport at the grain boundary by Pezzotti *et al*. [13]. However, if higher strains in the range of 1% are involved, a linear stress-strain rate relationship can not be expected any longer. Highly localized strain fields are observed at grain boundaries in crept specimens of Si_3N_4 which were frozen under stress. In TEM investigations strain whorls were observed, located along grain boundaries. They appeared to be asymmetrical with respect to the grain boundary normal. The contours of the whorls appeared to originate from a single point contact between neighboring grains [22, 23]. Such point contacts cause nonlinear force-displacement relationship with a stress exponent >1 even if isotropic, homogenous, elastic material properties are assumed as shown by the equations of Hertz. However, the stress exponent in the constitutional equation for the anelastic deformation cannot be determined from the creep recovery curves without the assumption that primary creep deformation is completely recoverable. This is true only under the assumption that microstructural changes during the deformation can be neglected. After extremely high strains, attained during superplastic deformation, grain alignment caused by grain rotation, and grain elongation were observed [24]. It is assumed that such microstructural changes do not have to be taken into consideration because the overall strains are very small. However, the comparison of the curves in Fig. 11 shows that the model is not suitable to describe long-time deformation behavior because after 100 hours a hardening of the material was observed but not considered in the model. The activation energy Q_3 calculated for the recoverable deformation is close to the activation energy Q_1. Therefore it can be assumed that the same deformation mechanisms are responsible for both recoverable and non-recoverable deformation.

Acknowledgement

In this paper results are presented, which were obtained at the International Cooperative Research Project Ceramic Superplasticity during a stay of the principal author as a guest researcher. This stay was enabled by an STA (Science and Technology Agency) Fellowship of the Japan Science and Technology Corporation and a Feodor-Lynen Fellowship of the Alexander von Humboldt Foundation. This support is gratefully acknowledged. The authors also thank I. Tanaka for the production of the material, J. Mayer, U. Eigenthaler, H. Labitzke, and U. Täffner for the microscopic investigations, and T. Nagano for his support during the mechanical testing.

References

1. W. A. SANDERS and D. M. MIESKOWSKI, *Ceramic Bulletin* **64**(2) (1985) 304.
2. J. HEINRICH and M. BÖHMER, *Ber. Dtsch. Keram. Ges.* **61**(8) (1984) 399.
3. J. L. ISKOE, F. F. LANGE and E. S. DIAZ, Effect of selected impurities on the high temperature mechanical properties of hot-pressed silicon nitride, *J. Mater. Sci.* **11** (1976) 908.
4. H.-J. KLEEBE, M. J. HOFFMANN and M. RÜHLE, *Z. Metallkd.* **83**(8) (1992) 610.
5. H.-J. KLEEBE, *J. Ceram. Soc. Jpn.* **105**(6) (1997) 453.
6. R. L. STOCKER and M. F. ASHBY, *Rev. Geophys. Space Phys.* **11** (1973) 391.
7. R. KOSSOWSKY, D. G. MILLER and E. S. DIAZ, *J. Mater. Sci.* **10** (1975) 983.
8. W. E. LUECKE, S. M. WIEDERHORN, B. J. HOCKEY, R. F. KRAUSE JR. and G. G. LONG, *J. Amer. Ceram. Soc.* **78**(8) (1995) 2085.
9. D. R. MOSHER, R. RAJ and R. KOSSOWSKY, *J. Mater. Sci.* **11** (1976) 49.
10. D. A. WOODFORD, *J. Amer. Ceram. Soc.* **81**(9) (1998) 2327.
11. I. TANAKA, G. PEZZOTTI, T. OKAMOTO, Y. MIYAMOTO and M. KOIZUMI, *ibid.* **72**(9) (1989) 1656.
12. H. GU, R. M. CANNON and M. RÜHLE, *J. Mater Res.* **13**(2) (1998) 376.
13. G. PEZZOTTI, K. OTA and H.-J. KLEEBE, *J. Amer. Ceram. Soc.* **79**(9) (1996) 2237.
14. M. BACKHAUS-RICOULT, P. EVENO, J. CASTAING and H.-J. KLEEBE, in "High Temperature Creep Behavior of High Purity Hot-Pressed Silicon Nitride, Plastic Deformation of Ceramics," edited by R. C. Bradt *et al*. (Plenum Press, New York, 1995) p. 555.
15. D. C. CRANMER, B. J. HOCKEY and S. M. WIEDERHORN, Creep and Creep Rupture of HIP'ed Si_3N_4, *Ceram. Eng. Sci. Proc.* **12**(9/10) (1991) 1862.

16. W. E. LUECKE, personal communication.
17. F. F. LANGE, B. I. DAVIS and D. R. CLARKE, *J. Mater. Sci*. **15** (1980) 601.
18. G. BREBEC, R. SEGUIN, C. SELLA, J. BEVENOT and J. C. MARTIN, *Acta Metall*. **28** (1980) 327.
19. K. EGUCHI, in "Glass Handbook" edited by S. Sakka, T. Sakaino and K. Takahashi (Asakura Shoten, Tokyo, Japan, 1977) p. 98.
20. M. OHASHI, M. TATEDA, K. TAJIMA and K. SHIRAKI, *Electron Lett*. **28** (1992) 1008.
21. F. F. LANGE, B. I. DAVIS and D. R. CLARKE, *J. Mater. Sci*. **15** (1980) 616.
22. F. F. LANGE, D. R. CLARKE and B. I. DAVIS, *J. Mater. Sci*. **15** (1980) 611.
23. P. BURGER, R. DUCLOS and J. CRAMPON, *Mater. Sci. Eng.* **A222** (1997) 175.
24. N. KONDO, E. SATO and F. WAKAI, *J. Amer. Ceram. Soc*. **81**(12) (1998) 3221.

Received 28 September 1999
and accepted 28 September 2000